Electronic Supplementary Information

Large scale and oxygen vacancy 2D VO_2 porous thin sheets to enable high-performance zinc ion storage

Qingqing He, Huayu Wang, Mengda Xue, Yanxin Liao, Jie Bai and Lingyun Chen *

Department of Applied Chemistry, School of Chemistry and Chemical Engineering, Chongqing University, Chongqing 401331, China.

*E-mail: lychen@cqu.edu.cn

Contents

1. Experimental Procedures

1.1. Synthesis of VO_d

In this work, the chemicals (analytically pure) purchased from Aladdin Co., Ltd. (Shanghai, PR China).

Moreover, they are all used as preparation 2D nanosheets of vanadium dioxide with oxygen defect (O_d) engineeringby hydrothermal reaction based on a dissolution–recrystallization process.

In a typical procedure, V_2O_5 (Sigma-Aldrich, 1.1 g) was dispersed in 200 mL of 0.4 M citric acid solution under vigorous stirring 18 h, transferred to a 10 mL glass bottle, and kept in an oven at 80 °C for 24 h to form spongy aerogel. Then, the aerogel was dissolved into 100 mL deionized water and stirred for 15 min. After that, the aerogel was transferred to a hydrothermal reactor and heated at 210℃ for 14 h to obtain brown flakes. Finally, the as-synthesized product was thoroughly washed with distilled water and ethanol several times and dried at 80 °C for 12 h.

1.2. Material Characterization

The powder XRD patterns were measured using a Rigaku SmartLab X-ray diffractometer 9 kW equipped with a D/teX Ultra 250 detector operating at 45 kV and 200 mA using Cu Kα radiation (λ = 1.540593) within a scanning angle, 2θ, range of 5–90° in steps of 0.01° using the Bragg–Brentano geometry. The morphologies of the samples were examined by a field-emission scanning electron microscope (FE-SEM, Helios Nanolab 600i, FEI). The thermogravimetric analysis (TGA, SDTQ600) tests with a heating rate of 5°C min^{-1} from room temperature to 600 C under Air atmosphere were conducted to study the thermal behavior of samples. Field emission Transmission Electron Microscope (TEM, Thermo Fisher Scientific CDLtd). Fourier transform infrared (FTIR) (Thermo Fisher Scientific, Nicolet iS50). The porous structural parameters were collected via N_2 physisorption isotherms (BET, max-II). X-ray photoelectron spectroscopy (XPS) (ESCALAB 250, Thermo-VG Scientific) measurements were performed in macro mode (3 mm × 3 mm) to obtain information about the binding energy of the vanadium and valence band. The electron paramagnetic resonance (EPR) spectra were measured at 294 K with a Bruker EMX plus 10/12 (equipped with Oxford ESR910 Liquid Helium cryostat).

1.3. Electrochemical Measurements

Electrochemical experiments were performed using 2032-type coin cells within the voltage window of 0.2–1.8V using a metallic Zn foil as the counter electrode. The working electrode was composed of 70 wt % VO_d, 20 wt % acetylene black, and 10 wt % polyvinylidene difluoride binder and was coated on a titanium foil and dried in air at 80 °C for 12 h. The mass loading of active materials is ~1mg cm^{-2}, the coating thickness is between 20-30um. The working and counter electrodes were separated by a piece of cellulose separator. The electrolyte used was 3 M $Zn(CF_3SO_3)_2$ aqueous solution. The discharge/charge measurements were performed with a LAND battery testing system (CT3002A). Cyclic voltammograms (CV) and the electrochemical impedance spectra (EIS, frequencies from 100 kHz to 100 mHz) were tested on an electrochemical workstation (CHI600E). Wo btained spectra were analyzed by equivalent circuits using ZView2 electrochemical impedance software (Scribner Associates Inc.). All of the tests were measured at room temperature.

2. Supplementary Method

2.1. Calculation of Capacitive Contribution

Generally, the total capacity at a certain scan rate comes from two components: surface-induced cap

acitive processes and diffusion-controlled processes, as follows [1]:

$$i = av^b \qquad (\log(i) = log(a) + b\,log(v)) \tag{1}$$

The above equation represents the relationship between the peak current (i) and the scan rate (v), where a and b are adjustable parameters and the value of b ranges from 0.5 to 1. When b=1, it represents that the charge storage process is controlled by the redox reaction on the surface (capacitive contribution), while b is 0.5 indicates that the charge storage is controlled by ionic diffusion. The value of b can be quantified by the slope of the redox peak log(i) to log(v). And discussed in the previous report [2], the capacitance contribution at each scan rate was quantified further.

In addition, the current response at a fixed potential at a certain scan rate can be expressed as a capacitive (k_1v) and diffusion-controlled ($k_2v^{1/2}$) process, as shown below [3]:

$$i = k_1 v + k_2 v^{\frac{1}{2}} \tag{2}$$

where k_1v denotes the total capacitive contribution and $k_2v^{1/2}$ denotes the contribution of the diffusion-controlled process. At different scan rates, the potential is fixed and k_1 and k_2 remain constant, so the CV curves for different scan rates can be used to calculate k_1 and k_2 at different voltages. The area obtained by connecting the capacitance contributions at individual voltage point is the capacitive contribution at certain scan rate, and the ratio of its area to the area of the CV diagram is the ratio of the capacitive contribution.

2.2. Zn^{2+} ion diffusion coeficients

Discussion of the Galvanostatic Intermittent Titration Technique (GITT)

GITT analysis was applied to determine the Zn^{2+} ion diffusion coefficients (DZn^{2+}, $cm^2\ s^{-1}$), following the methodology described in refs. [4-6]. In GITT analysis, the transient voltage that is generated due to the application of a current pulse is monitored as a function of time. Before the GITT measurement, the assembled cell was first discharged/charged at 0.2 A g^{-1} for 1 cycles to obtain a stable state. The GITT test was conducted by applying a pulse current of 0.2A g^{-1} for 10 min followed by a rest time of 30 min at open circuit step to allow relaxation back to equilibrium. In general, pulse times range from 10 minutes to several hours, depending on the material and its kinetics. Electrode materials with fast reaction rates, i.e. with high diffusion coefficients require shorter time pulse times so as to avoid parasitic side reactions during the hold, once the primary redox reaction is complete. Because of the relatively fast charge behavior of both the VO_d systems, an 600 sec pulse duration was chosen. This was repeatedly applied until the discharge (charge) voltage reached 0.2 V (1.8V) vs. Zn.

$$D_{Zn^{2+}} = \frac{4}{\tau\pi}\left(\frac{n_M V_M}{S}\right)^2\left(\frac{dE_s}{dE_\tau}\right)^2 \tag{4}$$

Where τ is the constant current pulse duration (600 sec); n_M and V_M are the moles (mol) of VO_d and

molar volume ($cm^3\ mol^{-1}$), respectively. S is the electrode electrolyte interface area (cm^2) taken as the geometric area of the electrode; dEs and dEτ are the change in the steady state voltage and overall cell voltage after the application of a current pulse in a single step GITT experiment. A marked-up diagram of a selected single step of the GITT profile, including the iR drop during discharge, is shown below:

The value of RR is calculated as the following formula:

$$RR = \frac{IR}{i} \tag{5}$$

Where i is the current density for the GITT test, and IR is illustrated in **Figure S8.**

3. Supporting Figures and Tables

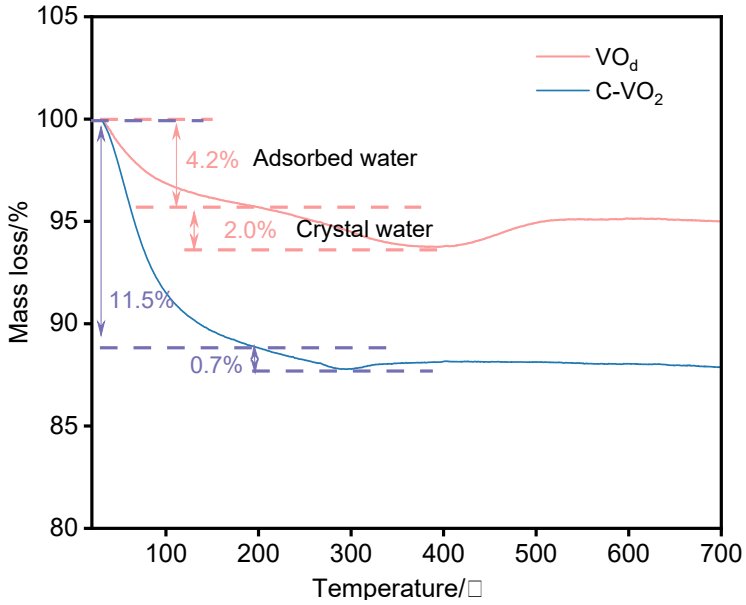

Figure S1. TGA of the C-VO_2 and VO_d

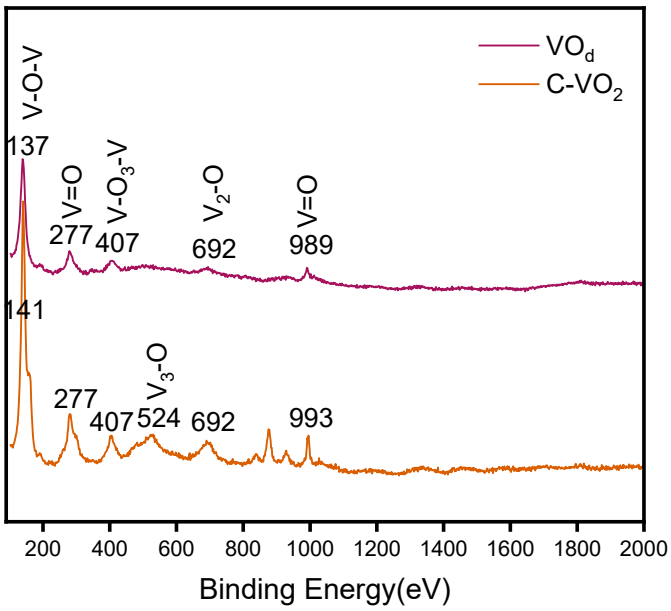

Figure S2. Raman of C-VO_2 and VO_d.

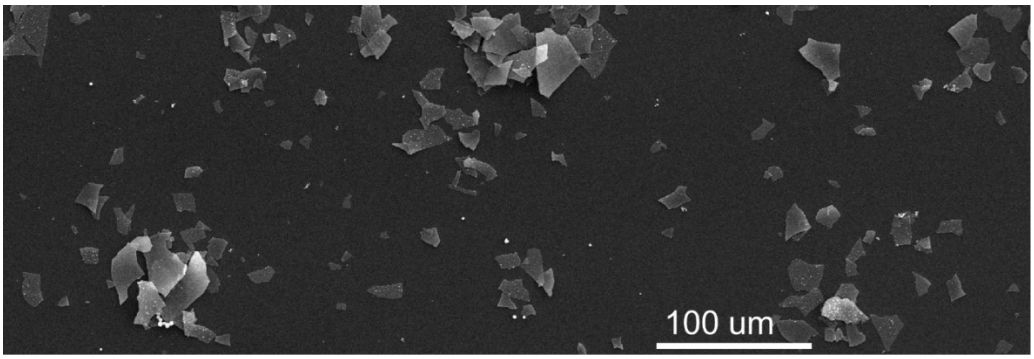

Figure S3. SEM of the VO_d.

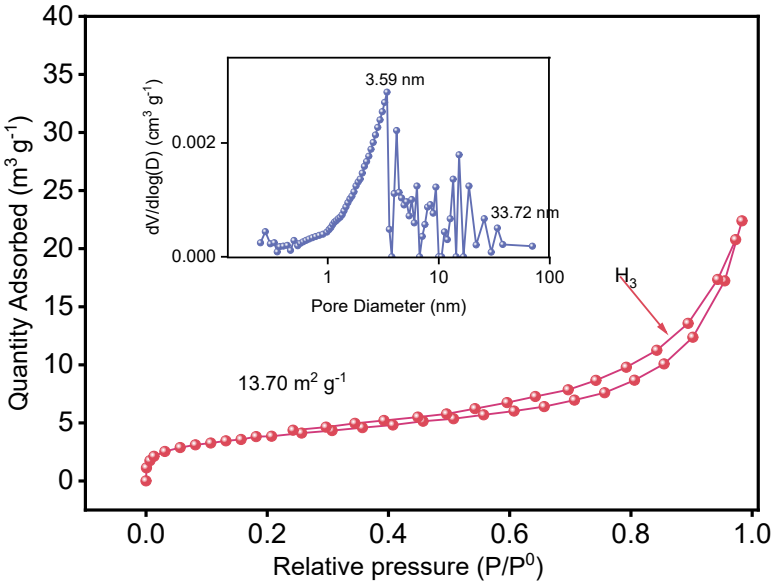

Figure S4. N_2 adsorption−desorption isotherms and pore size distributions (inset) of the VO_d.

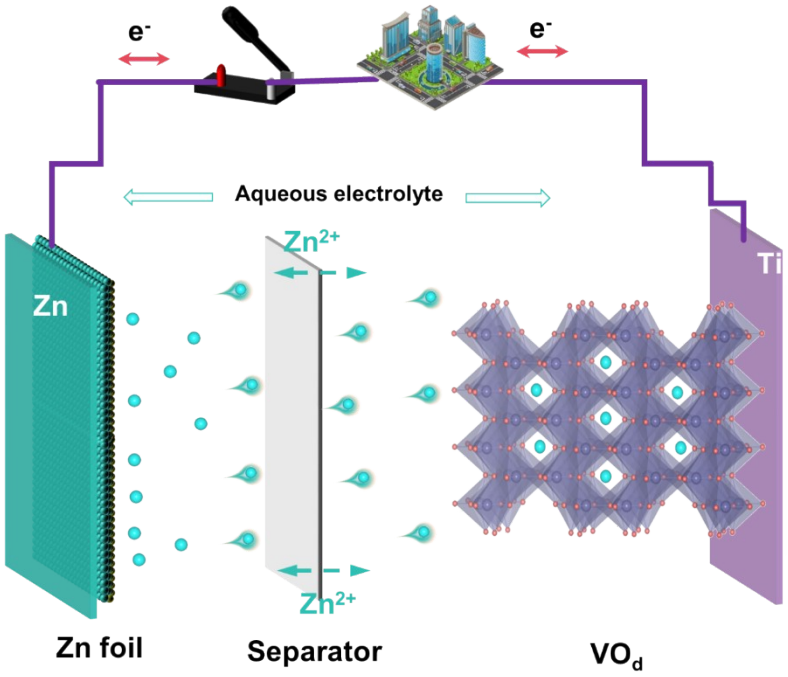

Figure S5. The schematic configuring of metallic VO_d //Zn AZIBs

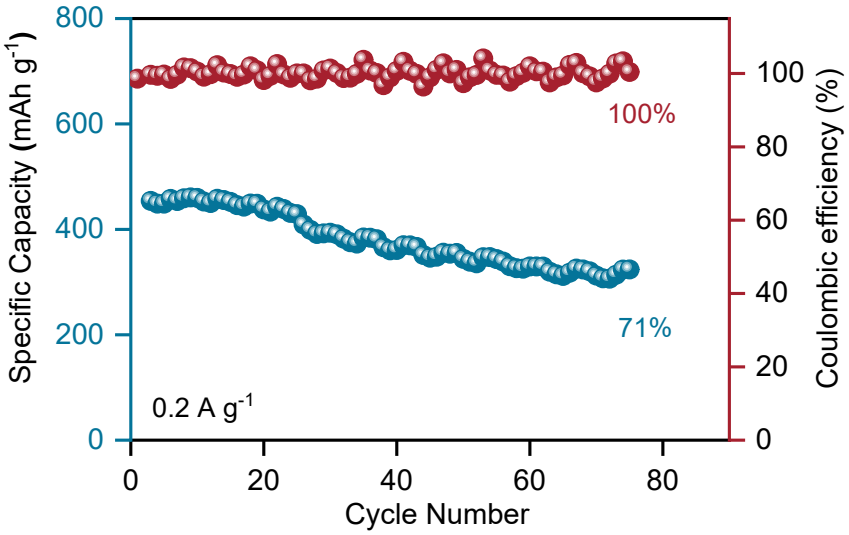

Figure S6. Cycling performance of VO_d at 0.2 A g^{-1}.

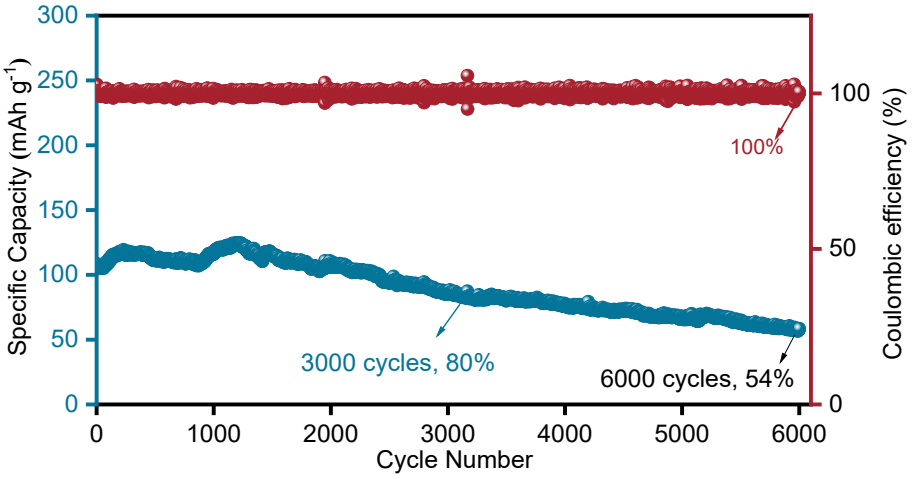

Figure S7. Cycling performance of VO_d at 10 A g^{-1} after 60000 cycles.

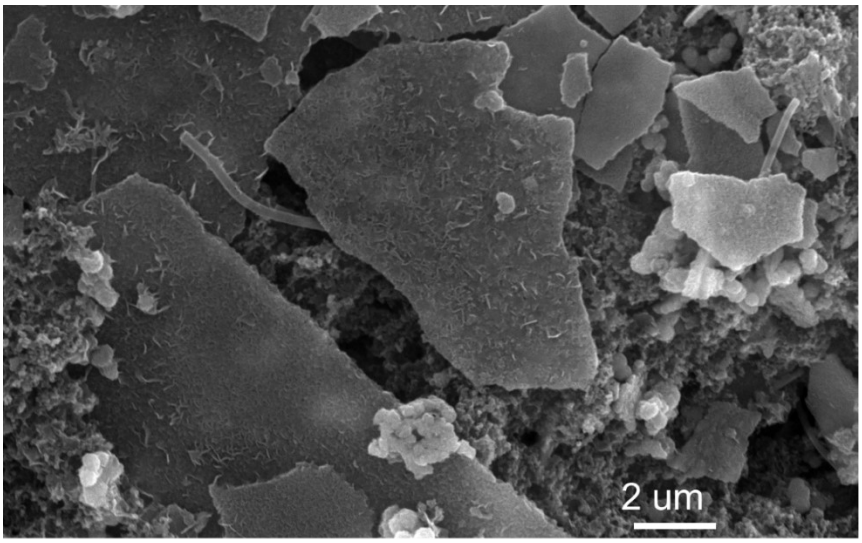

Figure S8. SEM of VOd after cycle 6000 times.

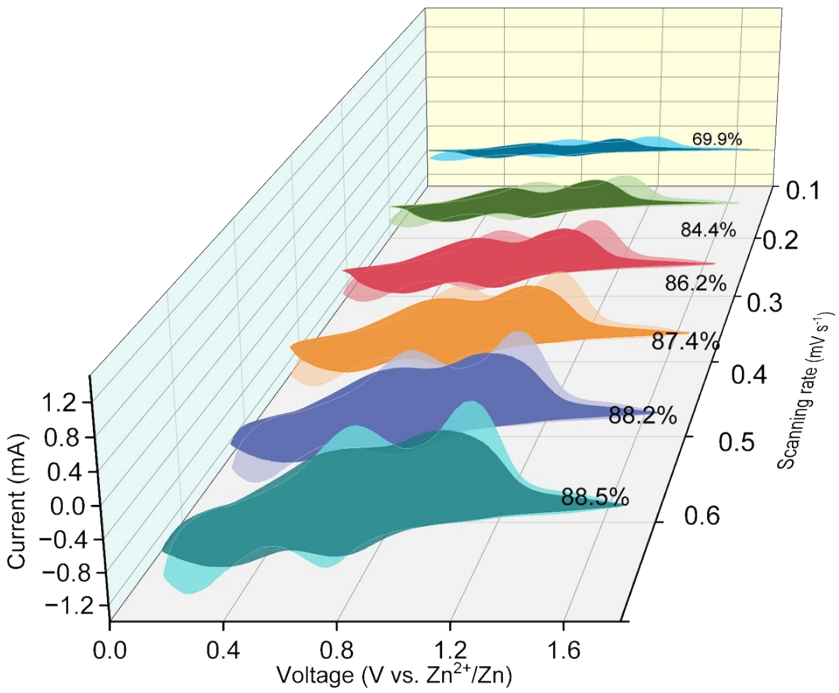

Figure S9. Capacitive contribution of the PMVO-sls cathode at 0.2-0.6 mV s^{-1}.

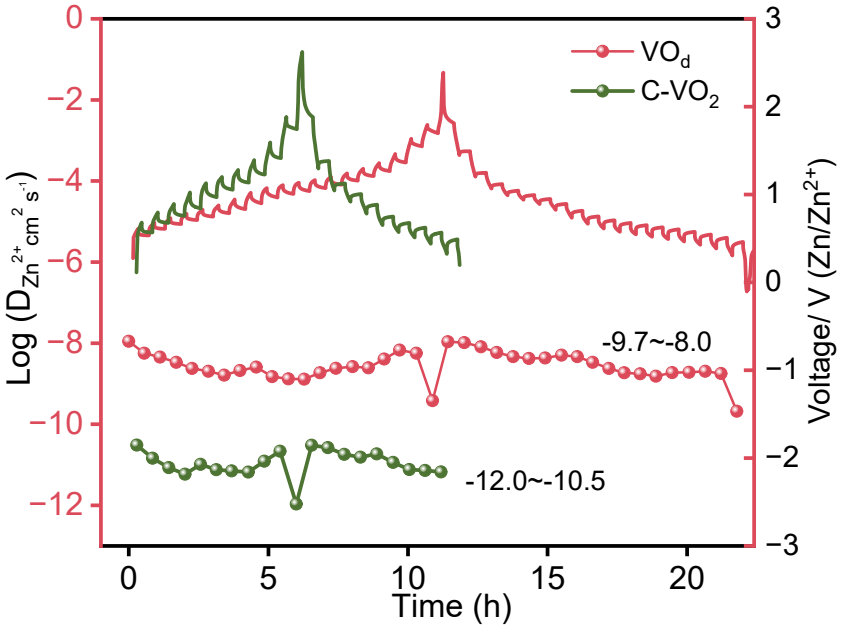

Figure S10. Diffusion coefficient distribution of the VO_d and C-VO_2 electrodes based on GITT charge/discharge profiles.

Table S1 The lattice parameters, cell volumes of the VOd.

Symmetry	Monoclinic			
Space group	C2/m (12)			
Lattice parameters	a = 12.057 Å	b = 3.697 Å	c = 6.416 Å	V= 275.46 Å^3
	α = 90°	β = 107°	γ = 90°	
Rp	3.69%			
Rf	3.68%			
Rwp	5.47%			
Rexp	5.38%			
Chi2(χ)	1.01			

Table S2 Comparison of electrochemical performance of VOd electrode versus state-of-the-art vanadate AZIBs cathode materials from literature

Catnode material	Current density（A g^{-1}）	Maximum specific capacity（mAh g^{-1}）	cycle performance	Ref.
cVO_2(B)	0.1	394		[7]
	3.0	83.9	81.2%, 1200 cycles	
Zn/VO_2@C-	0.1	400		[8]
0.5	5.0	193	1000 cycles	
VO_2(B)	0.1	249		[9]
	2.0	136	74%, 1000 cycles	
VO_{2-x}(B)	0.1	320	700 cycles	[10]
	3.0	150		
VO_2@V_2C	0.5	456		[11]
RGO/VO_2	0.1	276		[12]
	4.0	240	99%, 10000 cycles	
B-doped	0.1	281.7		[13]
VO_2 (B)	5.0	212.5	62.7%, 1000 cycles	
(Ni)VO_2	0.05	312		
	10.0	130	65.0%, 2000 cycles	[14]
O_d–HVO@P	0.2	337		
Py	10.0		77.2%, 1000 cycles	[15]
L-PANI-VO_2	4.0	290	58.6%, 1000 cycles	[16]
VO_d	0.2	457		This work
	10.0	110	80.0%, 3000 cycles	

Table S3 Charge transfer resisitance at different cycles of VOd in electrolyte.

Cycle number	Charge transfer resisitance (R_{ct},Ω)
0 (Pristine)	424.8
1	20.4
5	13.6
100	90.4

4. References

[1] C. Han, H. Li, Y. Li, J. Zhu, C. Zhi, Nat. Commun. 2021, 12, 1-12.

[2] Y. Tang, X. Li, H. Lv, D. Xie, W. Wang, C. Zhi, H. Li, Adv. Energy Mater. 2020, 10, 2000892.

[3] P. Li, Y. Wang, Q. Xiong, Y. Hou, S. Yang, H. Cui, Angew. Chem. Int. Ed., 62(23) (2023) e202303292.

[4] John Wang, Julien Polleux, James Lim, B. Dunn, J. Phys. Chem. C, 2007, 111, 14925-14931.

[5] D.W. Dees, S. Kawauchi, D.P. Abraham, J. Prakash, J. Power Sources, 189 (2009) 263-268

[6] Z. Shen, L. Cao, C.D. Rahn, C.-Y. Wang, J. Electrochem. Soc., 160 (2013) A1842

[7] Z. Cao, L. Wang, H. Zhang, X. Zhang, J. Liao, J. Dong, J. Shi, P. Zhuang, Y. Cao, M. Ye, J. Shen, P.M. Ajayan, Adv. Funct. Mater., 30 (2020) 2000472.

[8] Y. Liu, Y. Liu, X. Wu, Y.-R. Cho, ACS Appl. Mater. Interfaces, 14 (2022) 11654-11662.

[9] Q. Pang, H. Zhao, R. Lian, Q. Fu, Y. Wei, A. Sarapulova, J. Sun, C. Wang, G. Chen, H. Ehrenberg, J. Mater. Chem. A , 8 (2020) 9567-9578.

[10] W. Zhang, Y. Xiao, C. Zuo, W. Tang, G. Liu, S. Wang, W. Cai, S. Dong, P. Luo, ChemSusChem, 14 (2021) 971-978.

[11] J. Chen, B. Xiao, C. Hu, H. Chen, J. Huang, D. Yan, S. Peng, ACS Appl. Mater. Interfaces, 14 (2022) 28760-28768.

[12] X. Dai, F. Wan, L. Zhang, H. Cao, Z. Niu, Energy Storage Mater., 17 (2019) 143-150.

[13] S. Wang, H. Zhang, K. Zhao, W. Liu, N. Luo, J. Zhao, S. Wu, J. Ding, S. Fang, F. Cheng, Carbon Energy, 5 (2023) e330.

[14] Y. Cai, R. Chua, Z. Kou, H. Ren, D. Yuan, S. Huang, S. Kumar, V. Verma, P. Amonpattaratkit, M. Srinivasan, ACS Appl. Mater. Interfaces, 12 (2020) 36110-36118.

[15] Z. Zhang, B. Xi, X. Wang, X. Ma, W. Chen, J. Feng, S. Xiong, Advanced Functional Materials, 31 (2021) 2103070.

[16] X. Yuan, Y. Nie, T. Zou, C. Deng, Y. Zhang, Z. Wang, J. Wang, C. Zhang, E. Ye, ACS Appl. Energy Mater., 5 (2022) 13692-13701.